http://dx.doi.org/10.5012/bkcs.2011.32.11.4035

Photovoltaic Behavior of Dye-sensitized Long TiO_2 Nanotube Arrays

Sang Mo Kim, Hark Jin Kim, Yong Joo Kim, Gooil Lim, Young Sik Choi, and Wan In Lee*

*Department of Chemistry, Inha University, Incheon 402-751, Korea. *E-mail: wanin@inha.ac.kr*
Received August 25, 2011, Accepted September 20, 2011

Long TiO_2 nanotube (NT) arrays, prepared by electrochemical anodization of Ti foils, have been utilized as dye-adsorbing electrodes in dye-sensitized solar cells (DSCs). By anodizing for 1-24 hr and subsequent annealing, highly crystallized and tightly-adhered NT arrays were tailored to 11-150 μm lengths, ~90 nm inner-pore diameter and ~30 nm wall thickness. I-V curves revealed that the photovoltaic conversion efficiency (η) was proportional to the NT length up to 36 μm. Beyond this length, the η was still steadily increased, though at a much lower rate. For example, an η of 5.05% at 36 μm was increased to 6.18% at 150 μm. Transient photoelectron spectroscopic analyses indicated that NT array-based DSCs revealed considerably higher electron diffusion coefficient (D_e) and life time (τ_e) than those with TiO_2 nanoparticles (NP). Moreover, the electron diffusion lengths (L_e) of the photo-injected electrons were considerably larger than the corresponding NT lengths in all the cases, suggesting that electron transport in NT arrays is highly efficient, regardless of tube length.

Key Words : Dye-sensitized solar cells (DSC), TiO_2 nanotube arrays, Anodization, Electron diffusion, Photovoltaic conversion efficiency

Introduction

Dye-sensitized solar cells (DSCs) based on molecular dyes adsorbed on the surfaces of nanocrystalline TiO_2 films have attracted extensive attention due both to their low production cost in electricity and their relatively high photovoltaic conversion efficiency (η) over 11%.[1-5] Anatase phase TiO_2 nanoparticles (NPs) of 15-20 nm size normally have been used in the formation of dye-adsorbing electrodes in DSCs, since the thick TiO_2 layers with high porosity and large surface area can be achieved conveniently by simple screen printing and a subsequent calcination process. In regard to electron transport, however, the NP-based TiO_2 electrode is not the optimum structure, since it possesses numerous grain boundaries among the nanoparticles.

Since Gong and co-workers introduced the first generation TiO_2 nanotube (NT) arrays, various studies have been dedicated to their control.[6-11] Thus far, considerable progress has been achieved in tailoring pore diameter, wall thickness and tube length, as well as in controlling long range ordering. In fact, as Frank *et al.* and Jennings *et al.* have reported,[12-15] the NT array might be a more suitable architecture for the efficient charge collection than NP-based film, in several respects. First, electrons injected from dye molecules can be transported more efficiently through the TiO_2 conduction band (CB), because the cylindrical NT structure is fabricated with the minimized number of grain boundaries. Second, the straight and uniform pore channels with a large diameter can allow fast diffusion of electrolytes. Third, the incident light can be efficiently utilized due to its strong light-scattering effect. However, application of the NT array to DSC electrodes entails some drawbacks. First, only back-contact devices are available,[16-20] since NT arrays usually are formed on Ti foil and the unreacted Ti layer is used as the working electrode (WE). With back-illumination, a considerable portion of the incident light is scattered at the Pt-coated transparent conductive oxide (TCO) layer, and can also be absorbed by I^-/I_3^--based electrolytes. Ito *et al.* reported that the 9.9% of η measured by front-illumination was only 7.2% by back-illumination, suggesting an ~30% decrease.[21] Second, the surface areas of NT arrays are considerably smaller than those of NP-based films. Grimes et al. calculated the roughness factor of NT arrays, defined as the physical surface area of the film per projected area.[22-24] In comparing the theoretical roughness factor of the NP layers prepared from the 20 nm-sized NP, that of the NT array in the same thickness was only about 20%, suggesting that the amount of loaded dye is significantly smaller for NT arrays. Although this limitation can be overcome by increasing the length of NT, then the photo-injected electrons have to travel longer distances to collect electrons at the Ti electrode with increasing the NT length. Therefore, the understanding to the electron transport behavior for the long NT arrays will be crucial in designing the efficient electrode structures for DSC.

From the first utilization of NT arrays as dye-adsorbing DSC electrodes by Grimes *et al.*[11,25] a great number of studies have been reported. For example, there are several reports on the correlation of NT length to the photovoltaic properties of NT-based DSCs.[26-31] In early studies, short NTs of less than a few microns in length were applied, with an observed η of 1.1-3.3%.[21-32] Recently, Diau *et al.* controlled the NT lengths to 6-30 μm[17] and 15-57 μm,[18] and in these ranges η was monotonously increased up to 5.2% and 6.1%, respectively, reporting that the η enhancements were caused by the increases in the overall surface area of the NT arrays.

The photovoltaic behaviors of further longer NT arrays have not yet been reported, presumably because of the adhesion problem between NT arrays and metallic Ti substrates during crystallization process. In the present study, the adhesion problem was successfully solved by applying the specially-designed heating profile. Well-adhered NT arrays in the range of 11-150 μm length were successfully prepared, and their electron transport behaviors were systematically investigated.

Experimental Section

Titanium foils (Aldrich, 99.7% purity) of 0.127 mm thickness and 2 × 2 cm^2 area, pre-cleaned with ethanol and acetone several times, were utilized in the formation of NT arrays. 0.5 wt % ammonium fluoride (NH_4F, 98+%, Aldrich) in a mixture of ethylene glycol and H_2O (98:2 in volume) was used as the electrolyte solution. A platinum foil of 3 × 6 cm^2 area was used as the counter electrode (CE) of a home-made anodization system, the titanium foil being employed as the WE. During anodization, a constant voltage of DC 60 V was applied to the titanium foil for 1-24 hr at 25 °C,[32,33] while stirring with 150 rpm. For crystallization to the anatase phase, the as-prepared amorphous NT array was heated at 150 °C for 2 hr, followed by annealing at 500 °C for 3 hr. Length of the prepared NT was proportional to the anodization time.

For dye adsorption, the fabricated TiO_2 films were immersed in anhydrous ethanol containing 5 × 10^{-4} M N719 dye (Solaronix Co.),[32] and maintained for 24 hr at room temperature. Pt-sputtered FTO glass was used as the CE. The thickness of Pt layer was ~2 nm, and the transmittance at 500 nm was 72%. The electrolyte consisted of 0.4 M LiI, 0.6 M 1-butyl-3-methyl-imidazolium iodide (BMII, Merck Co.), 0.03 M I_2, 0.1 M guanidinium thiocyanate (GSCN, Aldrich Chemical Co.), and 0.5 M 4-*tert*-butylpyridine (TBP, Aldrich) in acetonitrile and valeronitrile (85:15 v/v).[34-36] The active area of the dye-coated TiO_2 film was 0.420 cm^2.

I-V measurements were performed using a Keithley model 2400 source measurement unit. A 300 W Xenon lamp (Spectra-Physics) was used as the light source, irradiating to the CE side of the fabricated DSC. The light intensity was adjusted using an NREL-calibrated Si solar cell equipped with a KG-5 filter for approximating AM 1.5G one sun light intensity. The incident photon to current efficiency (IPCE) spectra was measured using an IPCE system (PV Measurements, Inc.). The electron diffusion coefficient (D_e) and the electron lifetime (τ_e) were measured by a laboratory-made SLITMP equipment, which is described in detail elsewhere.[37-40]

Results and Discussion

Crystallized NT arrays are prone to be peeled off from the bottom Ti substrate, owing to the stress buildup at the interface during annealing process, and this tendency becomes more severe with increasing the tube length. In the present work, this adhesion problem was solved, as already mentioned, by applying a specially-designed heating profile. That is, the temperature increased from room temperature to 150 °C according to a ramping rate of 1 °C/min and maintained at that temperature for 2 hr in air. The temperature was further increased to 500 °C at the same ramping rate, and was kept for 3 hr in air. It was then cooled to room temperature at a rate of 1 °C/min. Pre-annealing treatment at 150 °C and very slow heating rate seem to alleviate the stress in the interface of the Ti substrate by reducing the crystallization rate of NT arrays.

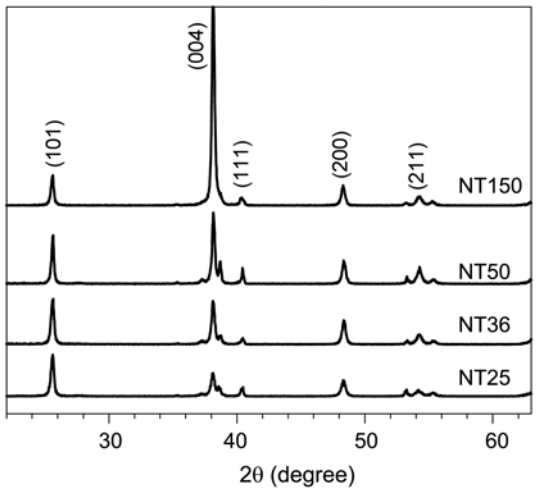

Figure 1. XRD patterns for several NT arrays annealed at 500 °C. NT25, NT36, NT50 and NT150 denote the NT arrays with the length of 25, 36, 50 and 150 μm, respectively.

Figure 1 shows the XRD patterns of NT arrays in different lengths, annealed at this heating profile. With increasing NT length the (004) peak becomes much more intense, whereas other peaks were not greatly influenced. This suggests that the TiO_2 grains in the NT arrays were more preferentially crystallized to the (004) direction during the annealing process. However, the crystallinity of the anatase grains was not appreciably dependent on the tube length. The average crystallite sizes, as determined by applying the Scherrer equation to the anatase (101) peaks, were 26-28 nm.

The SEM image in Figure 2(a) shows vertical-views of the crystallized NT arrays grown for several anodization hours. The length of the NT arrays grown for 4 hr was 25 μm, which was increased to 150 μm after 24 hr. Figure 2(b) plots the NT length as a function of the anodization time. The length of the NT arrays was proportional to the anodization time, suggesting that the anodization of Ti to TiO_2 proceeds at a constant rate of 6.2 μm/hr, regardless of nanotube length. Figure 2(c) shows the plan-view SEM image of the 150 μm-long TiO_2 NT arrays crystallized at 500 °C. The corresponding NT arrays were etched by about 100 μm using a reactive ion etching technique applying Cl_2 gas diluted in Ar as the etchant. Then its plan-view SEM image was monitored, as shown in Figure 2(d). The diameter and shape of the NT arrays were not appreciably changed, indicating clearly that the pore structures of the NT arrays

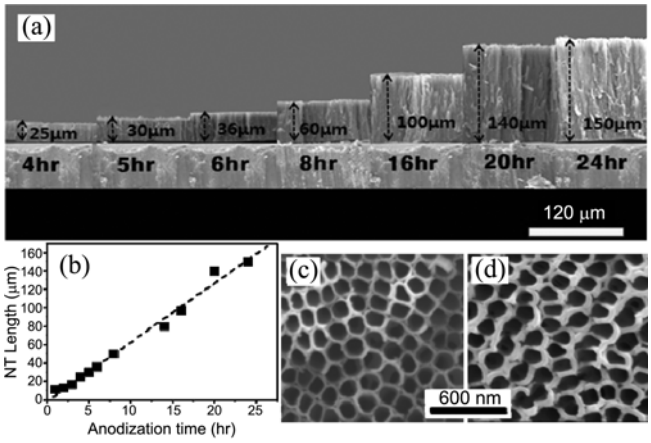

Figure 2. (a) Vertical-view SEM images of NT arrays of various lengths. (b) Plots of NT length *vs.* anodization time. Plan-view SEM images of (c) 150 μm-long NT arrays and (d) the corresponding sample etched by 100 μm. All of the NT arrays were annealed at 500 °C for 3 hr.

were quite uniform along the vertical direction. The outer diameter and wall thickness were ~150 nm and ~30 nm, respectively, suggesting that the pore diameter was ~90 nm.

The prepared 150 μm-thick NT arrays were also analyzed by TEM technique. Figure 3(a) shows the TEM image of a single NT, produced by ultrasonication of the 150 μm-thick NT arrays. The pore and outer diameters, as well as the wall thickness, were correspondent to those observed by SEM images. Figure 3(b) and 3(c) show the TEM images for a bundle of 150 μm-thick NT arrays, which are oriented parallel and perpendicular, respectively, to the pore channels. The individual pore diameters and wall thicknesses turned out to be quite uniform. Figure 3(d) shows the selected area electron diffraction (SAED) patterns, acquired from the whole area of the NT arrays (Figure 3(b)). It indicates that the prepared NT arrays were in the polycrystalline anatase phase.

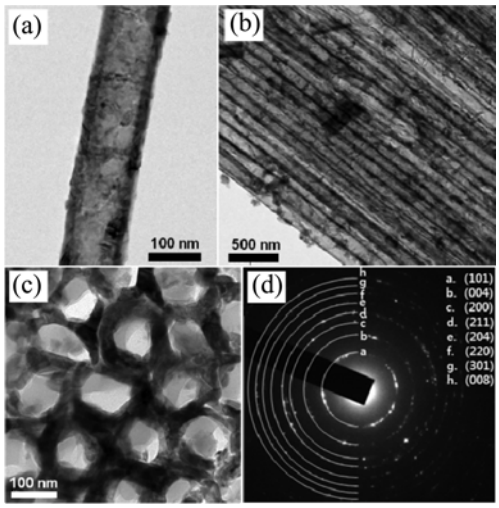

Figure 3. TEM images of (a) a single 150 μm-long NT and (b, c) a bundle of NT arrays monitored from the parallel and perpendicular directions, respectively, to the pore channels. (d) SAED patterns acquired from the whole area of (b).

In applications of NTs to DSCs, one of the major drawbacks is in their low surface area for dye molecule adsorption. To estimate the surface area of the several TiO_2 films per projected area, the roughness factors were evaluated, as proposed by Grimes *et al*.[11,19,29] The roughness factor of the 11 μm-long NT arrays was calculated to be only ~1/5 of the 10.2 μm-thick NP layer derived from 20 nm-sized TiO_2. This suggests that the length of NT arrays is required to be 50 μm to obtain similar surface area of 10 μm-thick NP film. Hence, the drawback of the low surface area in NT layers can be overcome with formation of very long tube arrays.

Figure 4(a) shows I-V curves for the back-illuminated DSCs constructed of several NT arrays in various lengths (DSC-NTs). By increasing the NT length, the short-circuit current density (J_{sc}) was steadily increased, whereas the open-circuit voltage (V_{oc}) was slightly decreased. The trends

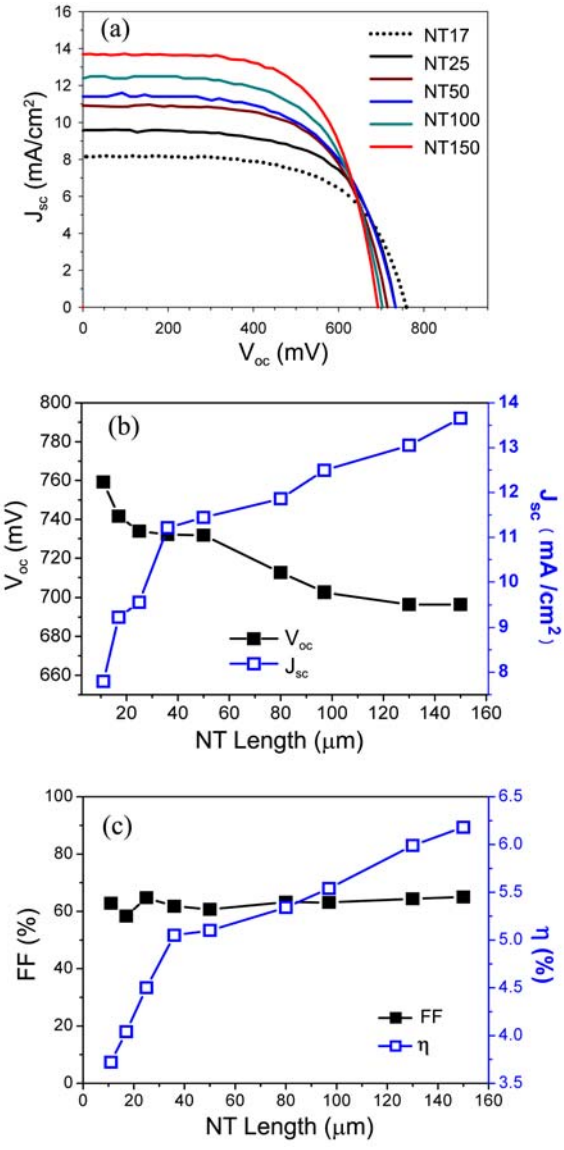

Figure 4. (a) I-V curves for back-illuminated DSCs constructed of several NT arrays in various lengths. (b) Plots of J_{sc} and V_{oc} as a function of NT length, and (c) those of *FF* and η *vs*. NT length.

of the photovoltaic properties as a function of NT length are more clearly described in Figure 4(b) and 4(c). It can be seen that J_{sc} values were increased proportionally in the 11-36 mm range. Beyond this range, the J_{sc} still steadily increased, but at a much lower rate. The slight decrease of V_{oc} with increasing NT length seemed to have originated from the higher possibility of the electron back reaction from the CB of TiO_2 to I_3^-, due to the increase in the surface area of the TiO_2 and the travel distance for the photo-injected electrons. Figure 4c also shows that the fill factor (*FF*) was not appreciably changed, irrespective of the tube length. The constant *FF* suggests that the electrical contact resistance between the NT array and the Ti substrate was not altered by increasing tube length, clearly indicating that tight adhesion had been maintained during the crystallization process, even for the 150 μm-long NT arrays. Accordingly, the η trend as a function of NT length was quite similar to that of J_{sc}: 5.05% at 36 μm was increased to 6.18% at 150 μm. Notably, even for the 150 μm-long NT arrays, the η seemed to increase steadily.

The electron diffusion coefficient (D_e) and the electron lifetime (τ_e) of the photo-injected electrons in the TiO_2 layer during DSC operation were analyzed by a stepped light-induced transient measurements of photocurrent (SLITMP) technique.[37-40] The electron diffusion coefficient was determined by the equation,

$$D_e = L^2 / (2.77 \times \tau_c),$$

where L and τ_c are the thickness of the TiO_2 layer and the time constant, respectively.[37] τ_c can be obtained by fitting the decay of transient photocurrent as a function of time (t) with a single-exponential function, $\exp(-t/\tau_c)$. Figure 5(a) plots the D_e as a function of the J_{sc} for the DSCs formed from NT arrays with various lengths. It was found that the D_e values gradually increased with the increase of the NT length. In principle, for the bulk TiO_2 layer, D_e is a constant value regardless of its dimension. In the DSC device, however, the photo-injected electrons travel through the TiO_2 layer and finally arrive at the TCO (or Ti for the NT) *via* the interface. Hence the determined D_e values for the thin TiO_2 layers will be underestimated due to the diffusion obstacle formed at the TiO_2/TCO interface. In order to obtain reasonable D_e values, therefore, the TiO_2 film thickness needs to be sufficiently high. In Figure 5(a), the D_e values of NTs were gradually increased, but the D_e of NT150 was only slightly higher than that of NT100. This suggests that the D_e value obtained for NT150 approaches to the bulk D_e of NT.

The electron lifetime (τ_e) also can be determined by fitting the decay of a transient photocurrent with $\exp(-t/\tau_e)$. Figure 5(b) plots the τ_e as a function of the J_{sc}, illustrating that the τ_e values increased with elongation of the NT arrays. In fact, with NT length ranging from 11 μm to 150 μm, the τ_e values increased by about one order. Compared with the τ_e of DSCs derived from the 20-nm-sized TiO_2 nanoparticle (DSC-NP), DSC-NTs offer remarkably higher τ_e values, as is consistent with the previous report .[12-14]

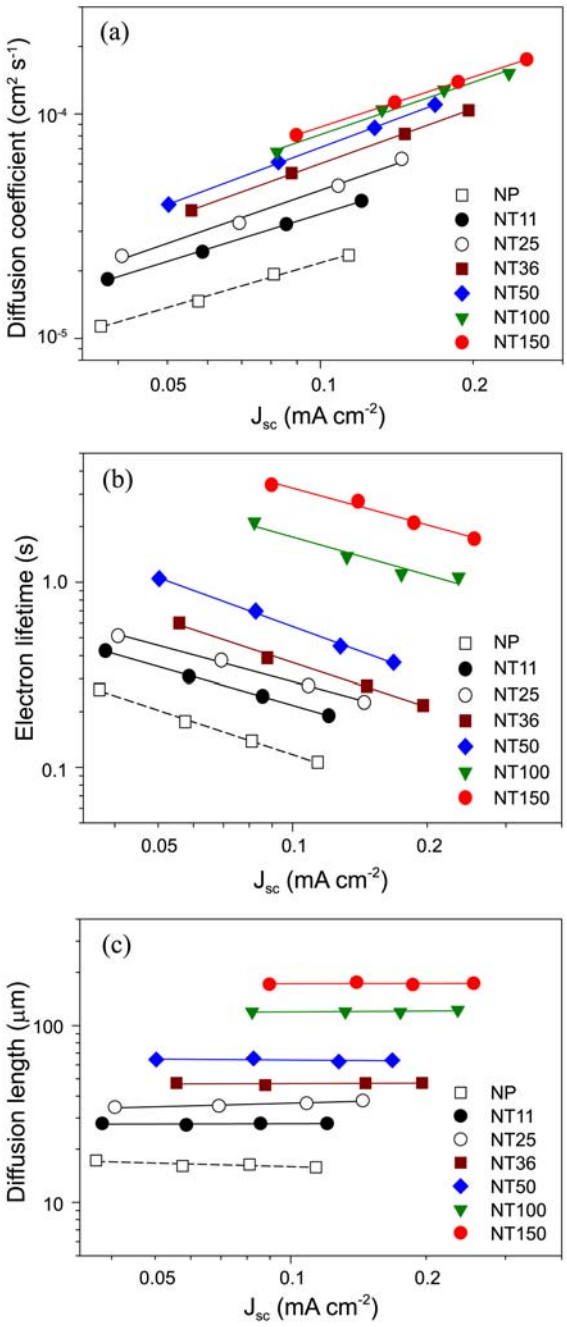

Figure 5. Plots of (a) electron diffusion coefficient (D_e) *vs.* J_{sc}, (b) the electron lifetime (τ_e) *vs.* J_{sc}, and (c) electron diffusion length (L_e) *vs.* J_{sc} for DSCs constructed of NT arrays in various lengths and 10.2 μm-thick NP film.

From the D_e and τ_e, the electron diffusion length (L_e) in the TiO_2 layer can be determined by the following equation.[40,41]

$$L_e = (D_e \times \tau_e)^{1/2}$$

Figure 5(c) provides plots of the calculated L_e *vs.* J_{sc} values for the DSC-NTs of various lengths. The L_e values of the DSC-NP and various DSC-NTs determined at the J_{sc} of 0.10 mA cm^{-2} are listed in Table 1. By Jennings *et al.* reported that L_e of TiO_2 NT was of the order of 100 μm by consider-

Table 1. Photovoltaic properties of DSCs derived from several TiO_2 photoelectrodes. DSC-NP-F and DSC-NP-B denote the front-illumination and back-illumination DSC-NPs, respectively. The electron diffusion length (L_e) values were determined at J_{sc} of 0.10 mA/cm^2

Samples	V_{oc} (mV)	J_{sc} (mA/cm^2)	FF (%)	η (%)	L_e (μm)
DSC-NP-F	821.628	11.893	73.28	7.16	16
DSC-NP-B	815.763	7.192	76.75	4.50	–
DSC-NT11	759.273	7.794	62.83	3.72	28
DSC-NT17	741.560	9.329	58.38	4.04	33
DSC-NT25	733.875	9.459	64.76	4.50	37
DSC-NT36	729.153	11.212	61.76	5.05	47
DSC-NT50	733.818	11.442	60.73	5.10	65
DSC-NT80	712.553	11.858	63.25	5.34	–
DSC-NT100	702.576	12.495	63.14	5.54	121
DSC-NT130	692.371	13.051	64.43	5.99	–
DSC-NT150	696.424	13.654	64.99	6.18	172

ing the difference between the electron quasi Fermi level in the DSC under short circuit and open circuit conditions.[15] The obtained L_e of 172 μm for the NT150 in the present work is consistent with their result.

The obtained L_e values of the DSC-NTs were remarkably higher than those of the DSC-NPs employing 10.2 μm-thick TiO_2 layer. For example, the L_e of DSC with 11 μm-long NT array was determined to be 28 μm, whereas that of DSC-NP in similar thickness was only 16 μm. Another notable observation here was that the electron diffusion lengths were relatively longer than the lengths of the corresponding NT arrays: the L_e of DSC-NT150 was 172 μm, and that of DSC-NT100 121 μm. This is a clear sign that the transport of photo-injected electrons through NT arrays is efficient even in the case of extremely long NT arrays. Therefore, η can be continuously increased with increasing the NT length. However, it was found that the V_{oc} gradually decreased with the increase of NT length, as shown in Figure 4(b). As NT length increases, both the surface area of the dye-adsorbing electrode and the average traveling distance of photo-injected electrons in the back-illuminated DSCs will increase linearly. It has been also known that L_e is required to be ~3 times of the TiO_2 film thickness to achieve the 98% collection efficiency.[15] Herein, for our long NTs in the range of 100-150 μm, L_e values were determined to be only 1.15-1.25 times of the corresponding NT lengths, as shown in Table 1. Thus, the probability of electron back-reactions to the electrolytes will be gradually increased with elongation of NT arrays, leading to the decrease of V_{oc}. This suggests that TiO_2 NT is not a perfect structure in transporting electrons from dyes to TCO, although it is much more efficient structure than the NP-based films.

For the purposes of a comparison, NP-based DSCs were fabricated and their photovoltaic properties were also analyzed. As shown in Table 1, the η of the DSC-NP as measured by front-illumination and back-illumination were 7.16% and 4.50%, respectively, indicating that the η was

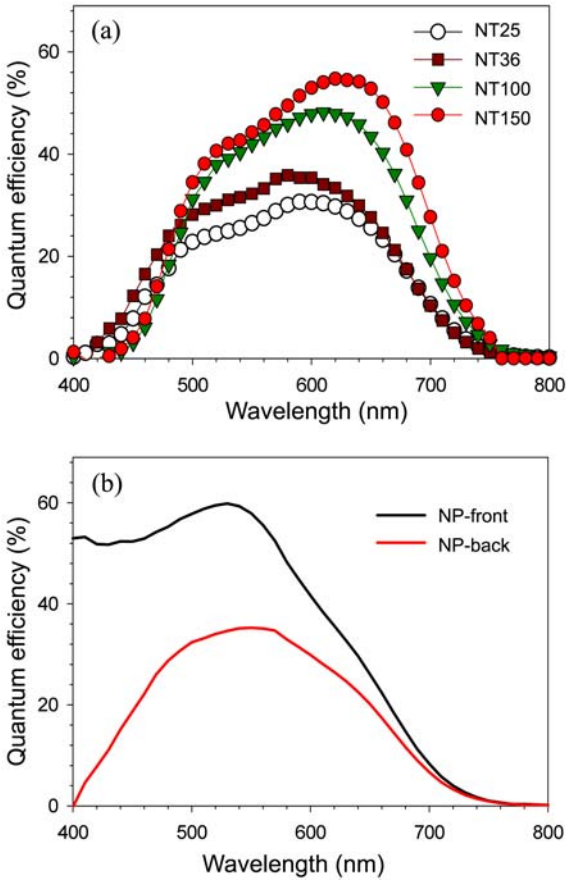

Figure 6. IPCE spectra for (a) several DSCs constructed of several NT arrays in various lengths and for (b) front-illuminated and back-illuminated DSC-NP (b) derived from 10.2 μm-thick NP film.

decreased to 63% by back-illumination. Thus, the achieved 6.18% cell efficiency for the back-illuminated DSC with the 150 μm-long NT is quite remarkable. The IPCE spectra of the several back-illuminated DSC-NTs are shown in Figure 6(a). With increasing NT length, the quantum efficiency (QE) values were gradually increased. At the same time, it was found that the QE maxima were shifted to longer wavelengths: the QE peak at 590 nm for DSC-NT25 was shifted to 630 nm for DSC-NT150. For the DSC-NP, the QE maximum of 60% by front-illumination fell to 35% by back-illumination. However, the peak position of ~550 nm was not changed at all, as shown in Figure 6(b), suggesting that the shift in the QE peak position was caused by the inherent scattering property of NT arrays. The considerable shift in the QE peak position for the DSC-NTs can be rationalized as follows. For the very long NT arrays, only the long-wavelength photons can arrive at the deep pores located near the Ti substrate, because most short-wavelength photons are scattered away and consumed by dye molecules at the NT pores close to the entrance. As a result, longer-wavelength light can be utilized more efficiently in generating electrons, with increasing NT length.

Therefore, the long NT arrays are considered to be an ideal charge-collecting electrode especially for the molecular dyes

responding to long-wavelength photons.

Conclusions

In the obtained results, the photovoltaic conversion efficiency (η) was linearly proportional to the length of NT up to 36 μm increasing at a rate of 0.05%/μm. Afterwards, this rate was lowered to 0.01%/μm, but the η continued to increase, even at 150 μm: the 5.05% η at 36 μm had been increased to 6.18% at 150 μm. The analysis with the SLITMP technique revealed that the electron diffusion distances (L_e) through the CB of the TiO_2 were longer than the lengths of the corresponding NTs. This clearly indicates that NT arrays, even the extremely long NT, are highly efficient structure in the electron transport. It was also found that that the light-utilizing efficiencies of NT-DSCs are higher than those of NP-DSCs owing to the stronger internal light-scattering effects of the NT arrays.

Acknowledgments. The authors gratefully acknowledge the financial support of Inha University and the Converging Research Center Program (2009-0082141) funded by the National Research Foundation, Korea.

References

1. O'Regan, B.; Grätzel, M. *Nature* **1991**, *353*, 737.
2. Kim, E. Y.; Lee, W. I.; Whang, C. M. *Bull. Korean Chem. Soc.* **2011**, *32*, 2671.
3. Grätzel, M. *Nature* **2001**, *414*, 338.
4. Pettersson, H.; Gruszecki, T. *Sol. Energy Mater. Sol. Cells* **2001**, *70*, 203.
5. O'Regan, B.; Lenzmann, F.; Muis, R.; Wienke, J. *Chem. Mater.* **2002**, *14*, 5023.
6. Varghese, O. K.; Gong, D. W.; Paulose, M.; Grimes, C. A.; Dickey, E. C. *J. Mater. Res.* **2003**, *18*, 156.
7. Zheng, Q.; Zhou, B. X.; Bai, J.; Cai, W. M.; Liao, J. S. *Prog. Chem.* **2007**, *19*, 117.
8. Tsuchiya, H.; Macak, J. M.; Taveira, L.; Balaur, E.; Ghicov, A.; Sirotna, K.; Schmuki, P. *Electrochem. Commun.* **2005**, *7*, 576.
9. Macak, J. M.; Tsuchiya, H.; Taveira, L.; Aldabergerova, S.; Schmuki, P. *Angew. Chem. Int. Ed*. **2005**, *44*, 7463.
10. Mor, G. K.; Varghese, O. K.; Paulose, M.; Grimes, C. A. *Adv. Funct. Mater.* **2005**, *15*, 1291.
11. Mor, G. K.; Shankar, K.; Paulose, M.; Varghese, O. K.; Grimes, C. A. *Nano Lett*. **2006**, *6*, 215.
12. Zhu, K.; Neale, N. R.; Miedaner, A.; Frank, A. J. *Nano Lett*. **2007**, *7*, 69.
13. Zhu, K.; Vinzant, T. B.; Neale, N. R.; Frank, A. J. *Nano Lett*. **2007**, *7*, 3739.
14. Wang, Q.; Zhu, K.; Neale, N. R.; Frank, A. J. *Nano Lett*. **2009**, *9*, 806.
15. Jennings, J. R.; Ghicov, A.; Peter, L. M.; Schmuki, P.; Walker, A. B. *J. Am. Chem. Soc.* **2008**, *130*, 13364.
16. Shankar, K.; Mor, G. K.; Prakasam, H. E.; Yoriya, S.; Paulose, M.; Varghese, O. K.; Grimes, C. A. *Nanotechnology* **2007**, *18*, 065707.
17. Chen, C.-C.; Chung, H.-W.; Chen, C.-H.; Lu, H.-P.; Lan, C.-M.; Chen, S.-F.; Luo, L.; Hung, C.-S.; Diau, E. W.-G. *J. Phys. Chem. C* **2008**, *112*, 19151.
18. Li, L.-L.; Tsai, C.-Y.; Wu, H.-P.; Chen, C.-C.; Diau, E. W.-G. *J. Mater. Chem.* **2010**, *20*, 2753.
19. Shankar, K.; Bandara, J.; Paulose, M.; Weitasch, H.; Varghese, O. K.; Mor, G. K.; LaTempa, T. J.; Thelakkat, M.; Grimes, C. A. *Nano Lett.* **2008**, *8*, 1654.
20. Kuang, D.; Brillet, J.; Chen, P.; Takata, M.; Uchida, S.; Miura, H.; Sumioka, K.; Zakeeruddin, S. M.; Grätzel, M. *ACS Nano.* **2008**, *2*, 1113.
21. Ito, S.; Ha, M. C.; Rothenberger, G.; Liska, P.; Comte, P.; Zakeeruddin, S. M.; Pechy, P.; Nazeeruddin, M. K.; Grätzel, M. *Chem. Commun*. **2006**, 4004.
22. Paulose, M.; Prakasam, H. E.; Varghese, O. K.; Peng, L.; Popat, K. C.; Mor, G. K.; Desai, T. A.; Grimes, C. A. *J. Phys. Chem. C* **2007**, *111*, 14992.
23. Varghese, O. K.; Gong, D.; Paulose, M.; Ong, K. G.; Dickey, E. C.; Grimes, C. A. *Adv. Mater.* **2003**, *15*, 624.
24. Mor, G. K.; Shankar, K.; Paulose, M.; Varghese, O. K.; Grimes, C. A. *Nano Lett.* **2005**, *5*, 191.
25. Mor, G. K.; Carvalho, M. A.; Varghese, O. K.; Pishko, M. V.; Grimes, C. A. *J. Mater. Res.* **2004**, *19*, 628.
26. Prakasam, H. E.; Shankar, K.; Paulose, M.; Varghese, O. K.; Grimes, C. A. *J. Phys. Chem. C* **2007**, *111*, 7235.
27. Kim, D.; Ghicov, A.; Schmuki, P. *Electrochem. Commun*. **2008**, *10*, 1835.
28. Chen, C. C.; Jehng, W. D.; Li, L.-L.; Diau, E. W.-G. *J. Electrochem. Soc*. **2009**, *156*, C304.
29. Park, J. H.; Lee, T.-W.; Kang, M. G. *Chem. Commun*. **2008**, 2867.
30. Chen Q.; Xu, D. *J. Phys. Chem. C* **2009**, *113*, 6310.
31. Tao, J.; Zhao, J.; Tang, C.; Kang, Y.; Li, Y. *New J. Chem*. **2008**, *32*, 2164.
32. Shankar, K.; Mor, G. K.; Prakasam, H. E.; Yoriya, S.; Paulose, M.; Varghese, O. K.; Grimes, C. A. *Nanotechnology* **2007**, *18*, 065707.
33. Nakade, S.; Kanzaki, T.; Wada, Y.; Yanagida, S. *Langmuir* **2005**, *21*, 10803.
34. Ahn, K. S.; Kang, M. S.; Lee, J. K.; Shin, B. C.; Lee, J. W. *Appl. Phys. Lett*. **2006**, *89*, 13103.
35. Kang, S.H.; Choi, S.-H.; Kang, M.-S.; Kim, J.-Y.; Kim, H.-S.; Hyeon, T.; Sung, Y.-E. *Adv. Mater.* **2008**, *20*, 54.
36. Ahn, K.-S.; Kang, M.-S.; Lee, J.-W.; Kang, Y. S. *J. Appl. Phys.* **2007**, *101*, 84312.
37. Krüger, J.; Plass, R.; Grätzel, M.; Cameron, P. J.; Peter, L. M. *J. Phys. Chem. B* **2003**, *107*, 7536.
38. Paulose, M.; Shankar, K.; Yoriya, S.; Prakasam, H. E.; Varghese, O. K.; Mor, G. K.; Latempa, T. A.; Fitzgerald, A.; Grimes, C. A. *J. Phys. Chem. B* **2006**, *110*, 16179.
39. Zhu, K.; Vinzant, T. B.; Neale, N. R.; Miedaner, A.; Frank, A. J. *Nano Lett.* **2007**, *7*, 3739.
40. Nakade, S.; Kanzaki, T.; Kubo, W.; Kitamura, T.; Wada, Y.; Yanagida, S. *J. Phys. Chem. B* **2005**, *109*, 3480.
41. Gao, F.; Wang, Y.; Zhang, J.; Shi, D.; Wang, M.; Humphry-Baker, R.; Wang, P.; Zakeeruddin, S. M.; Grätzel, M. *Chem. Commun.* **2008**, 2635.